

POD analyses of PIV and hot wire velocity data in a cylinder wake

S.L. Tang^{1,2}, L.Djenidi¹, R.A. Antonia¹ and Y. Zhou²

¹School of Engineering,
 University of Newcastle, NSW 2308, Australia

²Shenzhen Graduate School
 Harbin Institute of Technology, Shenzhen 518055, P. R. China

Abstract

The Proper Orthogonal Decomposition (POD) method has become a well-established tool used for identifying coherent structures since first introduced by Lumley [1]. In the present paper, we will compare two PODs in a cylinder wake. One is carried out on Particle Image Velocimetry (PIV) data (hereafter denoted POD_{PIV}) and the other is performed on single hot-wire measurements (hereafter denoted POD_{HW}). It is revealed that both PODs capture well the large scale corresponding to the Karman vortex shedding. The results suggest that POD_{HW} provides a less unambiguous and more objective identification of smaller scales than POD_{PIV}. It is also found that the POD_{HW} energy distribution, when adequately normalized, collapses well with the 1D velocity spectrum.

Introduction

The Proper Orthogonal Decomposition (POD) method has become a well-established tool used for identifying large scale structures since it was first introduced by Lumley [1]. The basic idea of POD, when it is applied to a fluctuation flow field $u(x, t)$, is to project $u(x, t)$ onto an orthogonal coordinate system $\Phi(x)$ which maximizes the following expression

$$\frac{\langle [\Phi(x), u(x, t)]^2 \rangle}{[\Phi(x), \Phi(x)]} \quad (1)$$

In this expression, (f, g) is the L^2 inner product $((f, g) = \int_{\Omega} f(x)g^*(x)dx$, where Ω is the flow domain, and the asterisk denotes a complex conjugate); the operator $\langle \dots \rangle$ denotes an ensemble average. The projections are optimal in the sense that the first few projections capture most of the energy. It is achieved by solving the following integral equation

$$\int R_{ij}(x, x')\Phi_j(x')dx' = \lambda\Phi_i(x) \quad (2)$$

where R_{ij} is the two-point velocity correlation tensor

$$R_{ij}(x, x') = \langle u_i(x)u_j^*(x') \rangle \quad (3)$$

The solution to Eq. (2) can be found by the means of the Hilbert-Schmidt theory since the kernel of Eq. (2) is Hermitian symmetric and the flow field has finite kinetic energy (or mathematically speaking, square integrable).

For snapshot POD, [2] the integral equation becomes

$$U^T U v = \lambda v \quad (4)$$

where $U^T U$ is the two-point space-correlation tensor in matrix form given by the products of the fluctuation part of the velocity at different spatial locations, and λ are the eigenvalues and v the eigenvectors of $U^T U$. The variable U is generally arranged as

$$U = \begin{bmatrix} u_{i1}^1 & u_{i1}^2 & \cdots & u_{i1}^N \\ u_{i2}^1 & u_{i2}^2 & \cdots & u_{i2}^N \\ \vdots & \vdots & \cdots & \vdots \\ u_{iM}^1 & u_{iM}^2 & \cdots & u_{iM}^N \end{bmatrix} \quad (5)$$

where $i(=1,2,3)$ denotes the fluctuating part of each of the three velocity components. Index N is the number of snapshots (from 1, 2, ... N) and M is the positions of velocity vectors in a given snapshot (from 1, 2, ... M). Ordering the solutions of Eq. (5) according to the size of the eigenvalues λ^k , the POD modes can be calculated using

$$\Phi_k(x) = \frac{1}{\sqrt{\lambda_k}} A v_k \quad (6)$$

where the first few modes are normally assumed to be the most energetic modes. Projecting the fluctuating field $u(x)$ onto the POD modes, we can obtain the POD coefficients that express the importance of the different modes.

$$a_k(t) = \Phi_k^T(x)u(x, t) \quad (7)$$

POD_{HW}

Because of the high-frequency response and fine spatial resolution of the hot-wire anemometer, it is ideal for the detailed study of turbulent flows, or any flow in which multi-scale fluctuations are of interest. One question naturally arises. Can we perform the above snapshot POD method on single hot-wire measurements in order to identify the large structures? The difficulty is that there is not sufficient information about the flow fields to create a velocity correlation matrix $U^T U$ when performing the snapshot method on single hot-wire data. In order to overcome this difficulty, the original signals ($u(t) = u(t_1), u(t_2), u(t_3), \dots, u(t_N), u(t_{N+1}), \dots$) measured by a single hot-wire are arranged as follows

$$U = \begin{bmatrix} u(t_1) & u(t_2) & \cdots & u(t_K) \\ u(t_2) & u(t_3) & \cdots & u(t_{K+1}) \\ u(t_3) & u(t_4) & \cdots & u(t_{K+2}) \\ \vdots & \vdots & \cdots & \vdots \\ u(t_{N-1}) & u(t_N) & \cdots & u(t_{N+K-2}) \\ u(t_N) & u(t_{N+1}) & \cdots & u(t_{N+K-1}) \end{bmatrix} \quad (8)$$

where $N \gg K$. The resulting matrix U has the following features:

- 1) The rms of each column in U are approximately equal.
- 2) Each column contains statistically the same information about every turbulent scale, i.e. the velocity spectra of all columns collapse.
- 3) The velocity correlation matrix is given by

$$R_{ij}(x, x+r) = \sum_{p=1}^N U_{pi}^T U_{pj} = \sum_{p=1}^N u(t_{p+i-1})u(t_{p+j-1}) \quad (9)$$

Once the velocity correlation matrix is formed, the rest of the POD analysis is the same as for the snapshot POD method, and thus will not be repeated.

Experimental details

Hot-wire Measurements were carried out in an open-return low-turbulence wind tunnel with a 2.2m long working section (0.35 m \times 0.35 m). A circular cylinder of $d=6$ mm in diameter was installed in the midplane and the measurement station is at $x/d=10$, $y/d=1$. Experiments were carried out at a free-stream velocity $U_\infty=10$ m/s, corresponding to a Reynolds number $Re = U_\infty d/\nu = 4000$, where ν is the kinematic viscosity of fluid.

PIV measurements were conducted in a closed circuit wind tunnel with a 5m long working section (0.8m \times 1.0m). A circular cylinder (diameter $d=10$ mm) was mounted horizontally across the working section. Experiments were carried out at a free-stream velocity $U_\infty=8.7$ m/s, corresponding to a Reynolds number $Re = U_\infty d/\nu = 5800$. A DANTEC standard PIV system was used to measure the instantaneous flow field, which was seeded by smoke, generated from paraffin oil, the averaged particle size being around 1 μ m in diameter. Flow illumination was provided by two pulse laser sources of a 532 nm wavelength. The view window of the camera covers the area of $x/d=4-15$ and $y/d=-3$ to 3 which represents the typical near-wake of a cylinder. A total of 2000 PIV image pairs were obtained for each measurement plane.

Results

Fig. 1 shows the distribution of the contributions from the POD modes to the total energy. The first two modes contain most of the energy for both PODs, while the contribution from the higher modes is very small. After the first two modes, the energy percentage is practically zero. Thus, the first two POD modes of both PODs represent the large-scale strongly coherent structures which dominate the flow field.

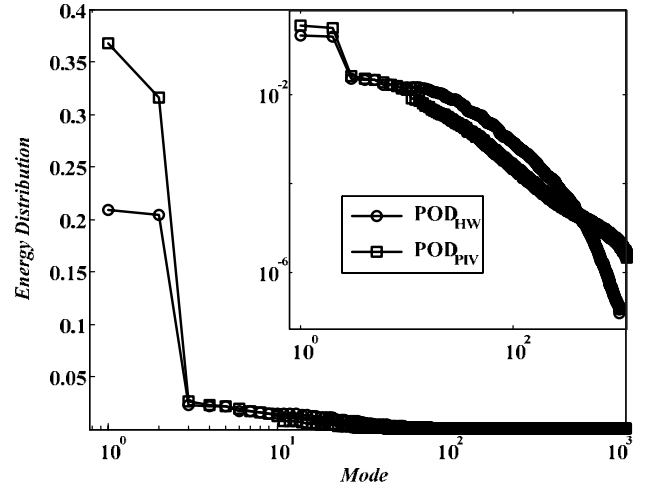


Figure 1. Percentage contribution of the POD modes to the total energy.

For a given flow field, the importance of the different modes can be expressed by the POD coefficients that are found by projecting the fields onto the POD modes as illustrated by (7). The relation between two modes can be shown as a scatter plot of the two coefficients. Fig. 2 and 3 show such scatter plots for the coefficients of the first two modes, a_1 and a_2 for both PODs. The scatter plot for the coefficients from POD_{PIV} shows a circular pattern in Fig. 2. Most points are located near a circle with radius 60 and centre at $(a_1, a_2) = (0, 0)$. The distribution of (a_1, a_2) from POD_{HW} shows a similar circular pattern but with a more perfect circular than that from POD_{PIV}. A possible reason that may contribute to this is due to the noise introduced by the PIV technique. The circular patterns indicate a strong connection between POD modes 1 and 2, which contain most of the energy and represent the large scale corresponding to the Karman vortex shedding frequency for both PODs.

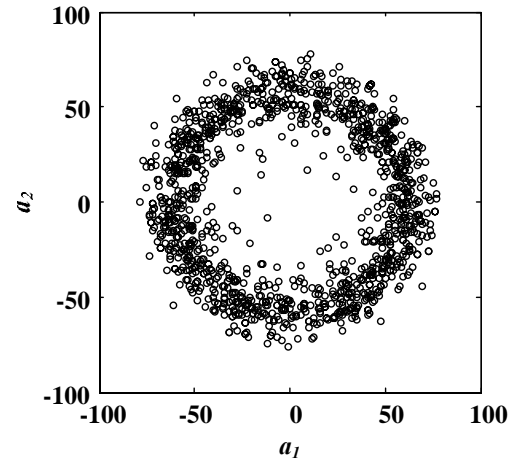


Figure 2. POD coefficients of the first two modes from POD_{PIV}.

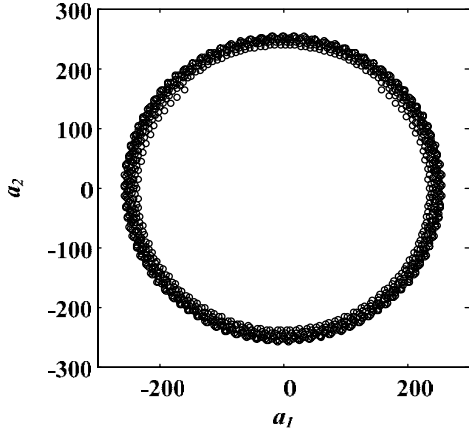


Figure 3. POD coefficients of the first two modes from POD_{HW}

The first mode is shown for both PODs in Fig. 4 (for POD_{PIV} , only u is shown). The present POD_{PIV} (Fig. 4a) mode is in good agreement with that of Feng et al. [3], presenting a pattern of alternating regions of positive and negative velocity values along $y/d=\pm 1$, which reflects the organized nature of the Karman vortex-street in the near-wake. Similar patterns can also be observed in Fig. 4b on POD_{HW} . The averaged vortex wavelength $\lambda_c=U_c/f_s$, (U_c is the convection velocity taken to be equal to $0.86U_\infty$ and f_s is the vortex shedding frequency at $x/d=10$ [4, 5]), is equal to $4.2d$, in good agreement with the value of $4.2d$ shown in the first mode of both PODs. The second mode for both PODs (not shown) has a similar pattern.

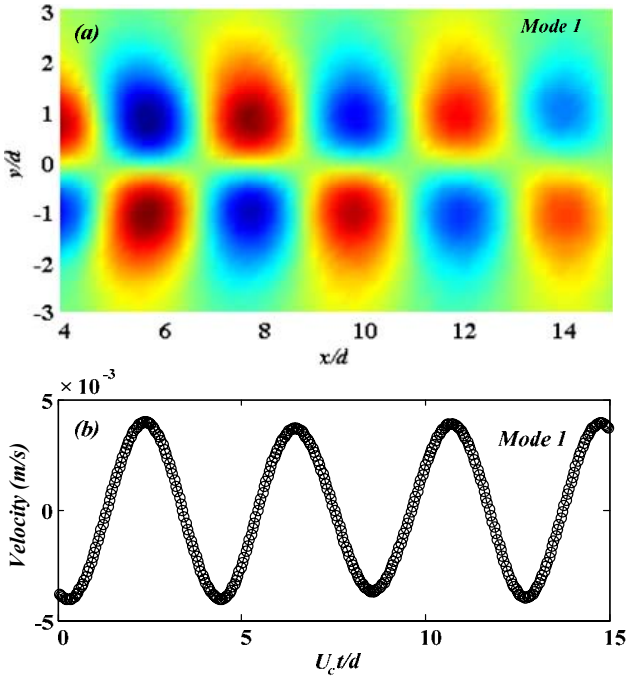


Figure 4. First POD mode. (a) POD_{PIV} ; (b) POD_{HW} .

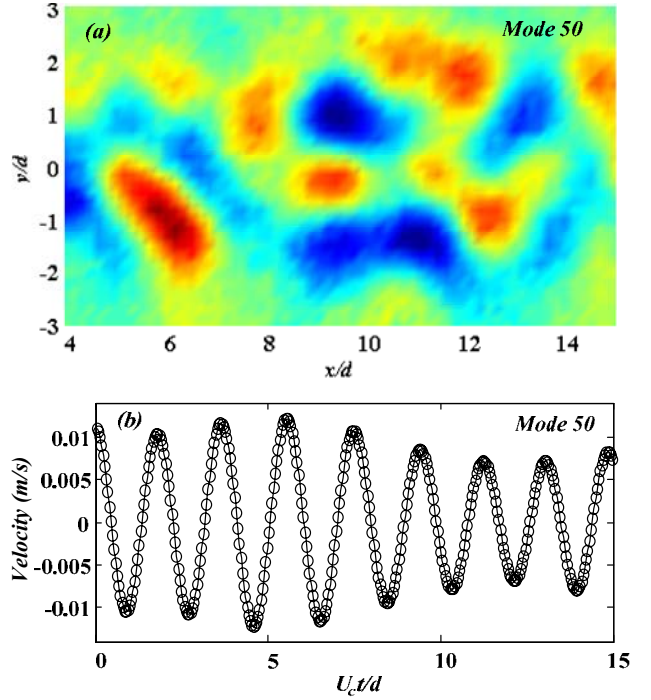


Figure 5. Fiftieth POD mode. (a) POD_{PIV} ; (b) POD_{HW} .

In contrast, the higher modes should be dominated by small-scale turbulent structures since the energy percentage contribution from the higher modes is very small (see Fig. 1.). For example, no coherent structure was found in the fiftieth mode for POD_{PIV} as shown in Fig. 5a. However, the same mode for POD_{HW} (Fig. 5b) shows a similar pattern as that for mode 1 although with a smaller wavelength. This means that POD_{HW} can identify not only the most energetic coherent structures, but also somewhat smaller structures. It is interesting to calculate the power spectrum of each mode for POD_{HW} . Fig. 6 shows clearly that the power spectrum of each mode exhibits one spike, reflecting that POD_{HW} has distinguished all turbulent scales effectively based on turbulent kinetic energy considerations. This can be further validated by the relation between modes and corresponding peak frequency for POD_{HW} as shown in Fig. 7.

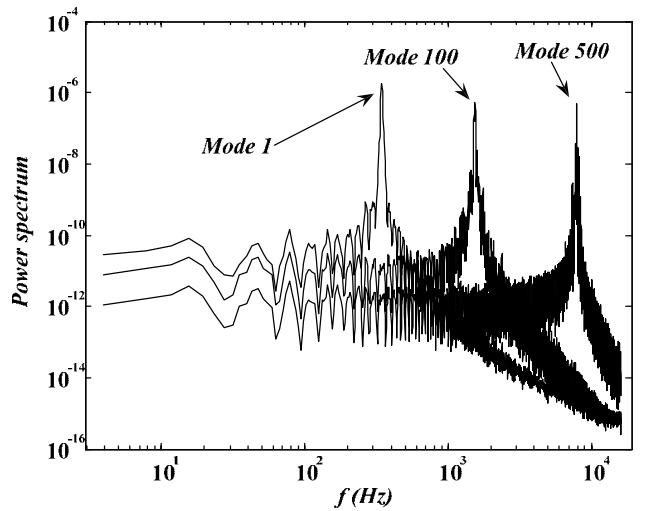


Figure 6. Power spectrum of modes for POD_{HW} .

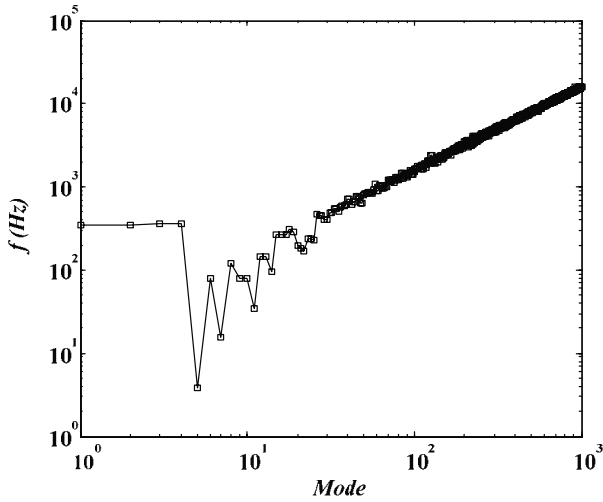


Figure 7. Peak frequency corresponding to Figure 6 vs modes.

Finally, the normalized POD energy distribution for POD_{HW} is plotted versus frequency corresponding to each mode in fig. 8. It is found that the normalized energy distribution collapses well with the 1D velocity spectrum, which further confirms that the POD_{HW} has distinguished all turbulent scales effectively.

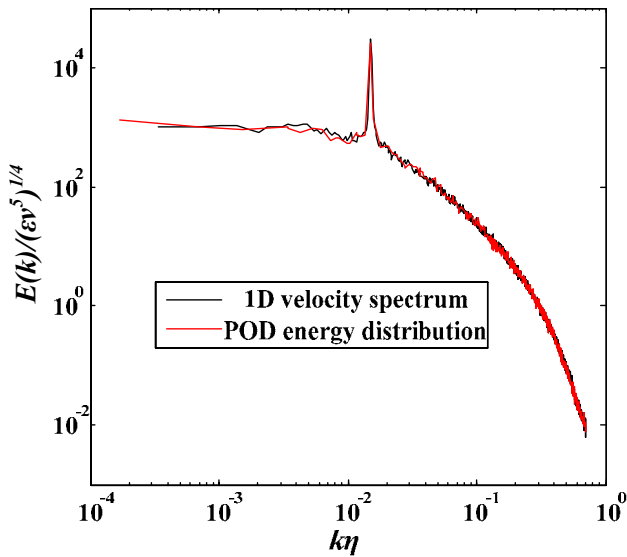


Figure 8. Normalized 1D velocity spectrum and POD energy distribution for POD_{HW} .

Conclusions

This paper has investigated the merits of using POD_{PIV} and POD_{HW} to aid in the identification of large structures in a near-wake of a cylinder. It is found that the dominant structures can be identified in the first two modes in both PODs. Furthermore, the results suggest that a more objective identification and description of smaller scales is provided more effectively by POD_{HW} than POD_{PIV} . The energy distribution for POD_{HW} , when adequately normalized, collapses well with the 1D velocity spectrum.

References

- [1] Lumley, J. L., The structure of inhomogeneous turbulent flows, in Atmospheric Turbulence and Radio Wave Propagation, edited by A. M. Yaglom and V. I. Tatarski Nauka, Moscow, 1967, p. 166.
- [2] Sirovich, L. 1987. Turbulence and the dynamics of coherent structures. Part I: Coherent structures, Q. Appl. Math. 45, 561
- [3] Feng L, H, Wang JJ, Pan C. 2011. Proper orthogonal decomposition analysis of vortex dynamics of a circular cylinder under synthetic jet control. Phys Fluids 23(1):014106
- [4] Zhou, Y., Zhang, H. J. & Yiu, M. W. 2002 The turbulent wake of two side-by-side circular cylinders. J. Fluid Mech . 458, 303–332.
- [5] Zhou, Y. & Antonia, R. A. 1992. Convection velocity measurements in a cylinder wake. Exps. Fluids 13, 63-70.